Inorganic Chemistry

Article

pubs.acs.org/IC

$Na_4La_2(CO_3)_5$ and $CsNa_5Ca_5(CO_3)_8$: Two New Carbonates as UV Nonlinear Optical Materials

Min Luo,[†,‡] GenXiang Wang,[§] Chensheng Lin,[†] Ning Ye,*[,†] Yuqiao Zhou,[†] and Wendan Cheng[†]

[†]Key Laboratory of Optoelectronic Materials Chemistry and Physics, Fujian Institute of Research on the Structure of Matter, Chinese Academy of Sciences, Fuzhou, Fujian 350002, P. R. China

[‡]University of Chinese Academy of Sciences, Beijing 100049, P. R. China

[§]College of Chemistry & Chemical Engineering, Fuzhou University, Shangjie town, Minhou county, Fuzhou, Fujian 350108, P. R. China

Supporting Information

ABSTRACT: Two nonlinear optical crystal carbonates ($Na_4La_2(CO_3)_5$ and $CsNa_5Ca_5(CO_3)_8$ were successfully synthesized by hydrothermal method, and both of them crystallized in the same noncentrosymmetric hexagonal space group *P*63*mc* (No. 186). The structure of $Na_4La_2(CO_3)_5$ consists of a three-dimensional network made up of $[CO_3]$ triangles as well as irregular $[Na_{0.67}La_{0.33}O_{10}]$ and $[NaO_8]$ polyhedra. The structure of $CsNa_5Ca_5(CO_3)_8$ can be described as the standing-on-edge $[CO_3]$ groups connect the adjacent infinite $[CaCO_3]_\infty$ layers in the *ab* plane to construct a framework with four types of channels running parallel to [010]. The Na, Cs, and $[Na_{0.67}Ca_{0.33}]$ atoms reside in these channels. The measurement of second harmonic generation (SHG) by the method adapted from Kurtz and Perry indicated that $Na_4La_2(CO_3)_5$ and $CsNa_5Ca_5(CO_3)_8$ were phase-matchable in the visible region and exhibited SHG responses of approximately 3 and 1 × KH_2PO_4 (KDP). Meanwhile, they exhibited wide transparent region with short UV cutoff edge at about 235 and 210 nm, respectively, suggesting that these crystals as NLO materials may have potential applications in the UV region.

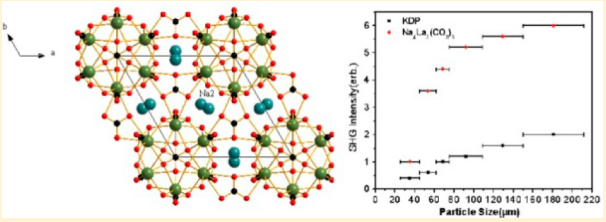

INTRODUCTION

Nonlinear optical (NLO) crystals[1−4] account for much for UV frequency conversion due to the increasing demand on the applications of UV laser. To obtain high NLO coefficients, wide UV transmittance, and useful materials, however, remain great challenges. Recently, borate-based UV NLO crystals[5−13] have been widely reported. Expanding the scope of NLO materials[14−17] is highly desired in both academic and industrial areas.

According to the anionic group theory,[18−20] the polar orientation of inorganic triangular groups that produce the large second-order susceptibility and birefringence, such as $[BO_3]^{3-}$ and $[CO_3]^{2-}$, have been proved as favorable structural units for designing NLO compounds. Numerous borates with the $[BO_3]^{3-}$ structural unit have been investigated: $KBe_2BO_3F_2$ (KBBF),[21] $Sr_2Be_2B_2O_7$ (SBBO),[22] $Ca_4GdO(BO_3)_3$ (GdCOB),[23] $YAl_3(BO_3)_4$ (YAB),[24−26] and recently several fluoride carbonates and carbonates, such as $ABCO_3F$ (A = K, Rb, Cs; B = Ca, Sr, Ba),[27] $K_{2.70}Pb_{5.15}(CO_3)_5F_3$,[28] $Na_8Lu_2(CO_3)_6F_2$, $Na_3Lu(CO_3)_2F_2$,[29] $CsPbCO_3F$,[30] and $Na_3Re(CO_3)_3$ (Re = Y, Gd),[31] were evidenced. The $[CO_3]^{2-}$ planar group with a high and anisotropic polarizability exists in calcite, in plane $\alpha_{\parallel} = 4.2 \times 10^{-24}$ cm^{-3}, and perpendicular $\alpha_{\perp} = 3.18 \times 10^{-24}$ cm^{-3}. In particular, if carbonate crystal with high $[CO_3]^{2-}$ density and $[CO_3]^{2-}$ groups coparallel aligned, large NLO effects can be realized. Thus, exploring carbonates as NLO materials from the perspective of structure−property relationships is very interesting.

Because of a low bond valence, $[CO_3]^{2-}$ anion groups do not polymerize. The layered habits usually exist in the crystal structures of carbonate, with $[CO_3]^{2-}$ slabs being interleaved with layers of large cations, predominantly alkaline, alkaline-earth, and rare-earth cations.[32−34] On the other hand, to ensure carbonate crystals with high transmission in UV, the metal cations with fully occupied d or f electron shells were used to explore the carbonate NLO crystals. In particular, the alkaline cations and alkaline earth cations are taken into account. In addition, trivalent rare-earth ions without unclosed d or f electrons are also expected in the carbonate NLO crystals, because the NLO materials that contain these rare-earth ions not only exhibited a wide transparent region but also may have larger second-harmonic-generation (SHG) responses that originated from a distorted rare-earth oxide polyhedron with large hyperpolarizability.[11]

Above all, when searching for new carbonates as UV NLO materials with excellent SHG properties, the carbonates containing alkaline, alkaline earth, or rare earth cations should be discovered by systematic investigation. On the basis of our exploration of carbonates of alkaline cations, alkaline earth cations, metals, and rare earth cations at the subcritical

Received: May 12, 2014
Published: July 16, 2014

   dx.doi.org/10.1021/ic501089f | *Inorg. Chem.* 2014, 53, 8098−8104

hydrothermal conditions, two novel noncentrosymmetric materials, $Na_4La_2(CO_3)_5$ and $CsNa_5Ca_5(CO_3)_8$, were found. Herein, we report the synthesis, characteristics of crystal structures, thermal behaviors, spectra, NLO properties, and the structure−properties relationship of these two carbonates.

EXPERIMENTAL SECTION

Reagents. Na_2CO_3 (99.8%), NaF (99.8%), $CaCl_2$ (99.0%), CsCl (99.0%) were purchased from Sinopharm. $La(NO_3)_3·6H_2O$ (99.0%) were purchased from Jinan Camolai Trading Company.

Synthesis. *Synthesis of $Na_4La_2(CO_3)_5$.* A mixture of Na_2CO_3 (2.12g, 0.02 mol), NaF (0.504g, 0.012 mol), $La(NO_3)_3·6H_2O$ (1.73 g, 0.004 mmol), and H_2O (5.0 mL) was sealed in an autoclave equipped with a Teflon liner (23 mL) and heated at 220 °C for 5 d, followed by slow cooling to room temperature at a rate of 3 °C/h. The reaction product was washed with deionized water and ethanol and then dried in air. Colorless hexagonal prism-shaped $Na_4La_2(CO_3)_5$ crystals were obtained as a single phase in a yield of about 80% based on La.

Synthesis of $CsNa_5Ca_5(CO_3)_8$. A mixture of Na_2CO_3 (2.12g, 0.02 mol), $CaCl_2$ (0.444g, 0.004 mol), CsCl (3.37 g, 0.02 mmol), and H_2O (10.0 mL) was sealed in an autoclave equipped with a Teflon liner (23 mL) and heated at 220 °C for 5 d, followed by slow cooling to room temperature at a rate of 3 °C/h. The reaction product was washed with deionized water and ethanol and then dried in air. Colorless hexagonal prism-shaped $CsNa_5Ca_5(CO_3)_8$ crystals were obtained as a single phase in a yield of about 75% based on Ca.

Single-Crystal X-ray Diffraction. Single-crystal X-ray diffraction data were collected at room temperature on a Rigaku Mercury CCD diffractometer with graphite-monochromatic Mo Kα radiation (λ = 0.710 73 Å). A transparent block of crystal was mounted on a glass fiber with epoxy for structure determination. A hemisphere of data was collected using a narrow-frame method with ω scan mode. The data were integrated using the CrystalClear program, and the intensities were corrected for Lorentz polarization, air absorption, and absorption attributable to the variation in the path length through the detector faceplate. Absorption corrections based on the Multiscan technique were also applied. The structures of $Na_4La_2(CO_3)_5$ and $CsNa_5Ca_5(CO_3)_8$ were solved by the direct methods using SHELXS-97.[35] During the refinement for $Na_4La_2(CO_3)_5$, owing to the large U(eq) and R values when these sites were assigned as La atoms, Na1 and La1 atoms were set to share the same sites. To retain charge balance, the molar ratio of La/Na was fixed to 0.67/0.33 in the disorder sites. Similar reasoning was applied in the case of compound $CsNa_5Ca_5(CO_3)_8$, when the occupancy ratios of Na/Ca were refined to be 0.67/0.33. At this stage of refinement, the U(eq) of the O(7) atom appeared to be very high. Consequently, the oxygen atom O(7) was split with a scale factor of 0.33. All thermal parameters were satisfying. To confirm the chemical composition of La/Na and Na/Ca in both compounds, we performed elemental analysis (see the Supporting Information, Table S5). In addition, all nonhydrogen atoms were refined with anisotropic thermal parameters. All of the structures were verified using the ADDSYM algorithm from the program PLATON,[36] and no higher symmetries were found. Relevant crystallographic data and details of the experimental conditions for $Na_4La_2(CO_3)_5$ and $CsNa_5Ca_5(CO_3)_8$ are summarized in Table 1. Atomic coordinates and isotropic displacement coefficients are listed in Tables S1 and S2 and bond lengths in Tables S3 and S4 in the Supporting Information.

Powder X-ray Diffraction. X-ray diffraction patterns of polycrystalline materials were obtained on a Rigaku Dmax2500 powder X-ray diffractometer by using Cu Kα radiation (λ = 1.540 598 Å) at room temperature in the angular range of 2θ = 5−65° with a scan step width of 0.05° and a fixed time of 0.2 s. The powder XRD patterns for the pure powder samples of $Na_4La_2(CO_3)_5$ (Figure 1) and $CsNa_5Ca_5(CO_3)_8$ showed good agreement with the calculated XRD patterns from the single-crystal models (see Figure S1 in the Supporting Information).

Table 1. Crystal Data and Structure Refinement for $Na_4La_2(CO_3)_5$ and $CsNa_5Ca_5(CO_3)_8$

formula	$Na_4La_2(CO_3)_5$	$CsNa_5Ca_5(CO_3)_8$
formula mass (amu)	669.83	928.34
crystal system	hexagonal	hexagonal
space group	*P*63*mc*	*P*63*mc*
a (Å)	10.55(2)	10.0845(5)
c (Å)	6.47(2)	12.7055(12
α (deg)	90	90
γ (deg)	120	120
V (Å^3)	624(3)	1119.00(13)
Z	2	2
ρ (calcd)(g/cm3)	3.567	2.755
temperature (K)	293(2)	293(2)
λ (Å)	0.710 73	0.710 73
F(000)	616	900
μ (mm^{-1})	7.00	3.02
θ (deg)	3.15−25.33	2.33−27.50
index range	$-12 \le h \le 10$	$-12 \le h \le 13$
	$-12 \le k \le 12$	$-13 \le k \le 12$
	$-7 \le h \le 7$	$-16 \le h \le 16$
Rint[a]	0.0761	0.0514
R/wR^a ($I > 2\sigma(I)$)	0.0542/0.1132	0.0296/0.0680
R/wR^a (all data)	0.0561/0.1148	0.0313/0.0693
GOF on F^2	1.230	1.124
absolute structure parameter	0.00(14)	0.00
largest diff. peak and hole (e/Å^{-3})	1.652 and −1.054	0.988 and −0.669

[a] $R(F) = \Sigma||F_o| - |F_c||/\Sigma|F_o|$. $wR(F_o^2) = [\Sigma w(F_o^2 - F_c^2)^2/\Sigma w(F_o^2)^2]^{1/2}$.

Elemental Analysis. Elemental analysis of the crystals was performed by using a Jobin Yvon Ultima2 inductively coupled plasma optical emission spectrometer (ICP-OES) with Sepex Certiprep standards. The crystal samples were dissolved in a mixture of nitric acid (3 mL) and hydrochloric acid (3 mL).

Thermal Analysis. The TG scans were measured on a NETZSCH STA 449C. Reference (Al_2O_3) and crystal samples (3−10 mg) were enclosed in Al_2O_3 crucibles and heated from room temperature to 1000 °C at a rate of 10 °C/min under a constant flow of nitrogen gas.

UV−vis Diffuse Reflectance Spectroscopy. UV−vis diffuse reflectance spectroscopy data were recorded at room temperature using a powder sample with $BaSO_4$ as a standard (100% reflectance) on a PerkinElmer Lamda-900 UV/vis/NIR spectrophotometer and scanned at 200−2500 nm. Reflectance spectra were converted to absorbance using the Kubelka−Munk function.[37,38]

Second-Harmonic Generation. Polycrystalline second-harmonic generation (SHG) signals were measured using the method adapted from Kurtz and Perry.[39] Since SHG efficiencies are known to depend strongly on particle size, polycrystalline samples were ground and sieved into the following particle size ranges: 25−45, 45−62, 62−75, 75−109, 109−150, and 150−212 μm. The samples were pressed between glass microscope cover slides and secured with tape in 1 mm thick aluminum holders containing an 8 mm diameter hole. To make relevant comparisons with known SHG materials, crystalline KDP was also ground and sieved into the same particle size ranges. The samples were then placed in a light-tight box and irradiated with a pulsed laser. The measurements were performed with a Q-switched Nd:YAG laser at 1064 nm and a frequency doubling at 532 nm, for visible and UV SHG. A cutoff filter was used to limit background flash-lamp light on the sample, and an interference filter (530 ± 10 nm) was used to select the second harmonic for detection with a photomultiplier tube attached to a RIGOL DS1052E 50-MHz oscilloscope. This procedure was then repeated using the standard NLO material KDP, and the ratio of the second-harmonic intensity outputs was calculated. No index-matching fluid was used in any of the experiment.

dx.doi.org/10.1021/ic501089f | Inorg. Chem. 2014, 53, 8098−8104

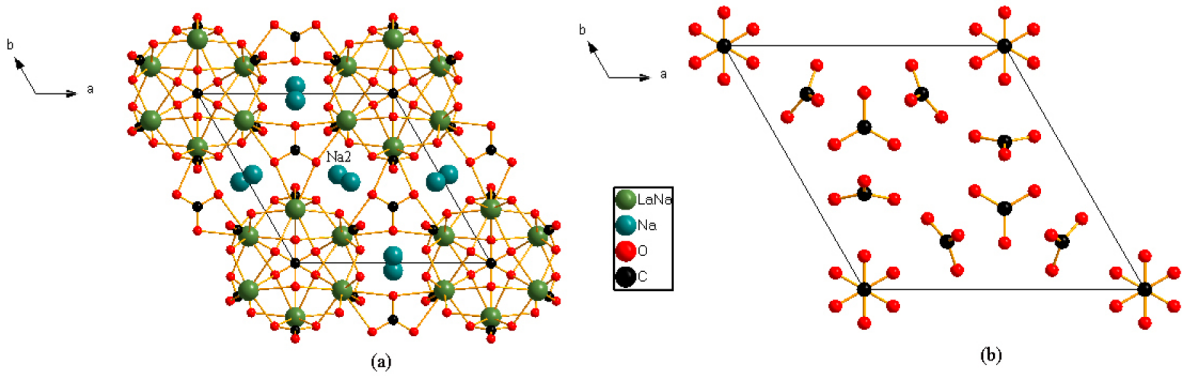

Figure 1. (a) View of the structure of $Na_4La_2(CO_3)_5$ down the *c* axis. (b) The "flat-lying" and "standing-on-edge" of $[CO_3]^{2-}$ groups in $Na_4La_2(CO_3)_5$.

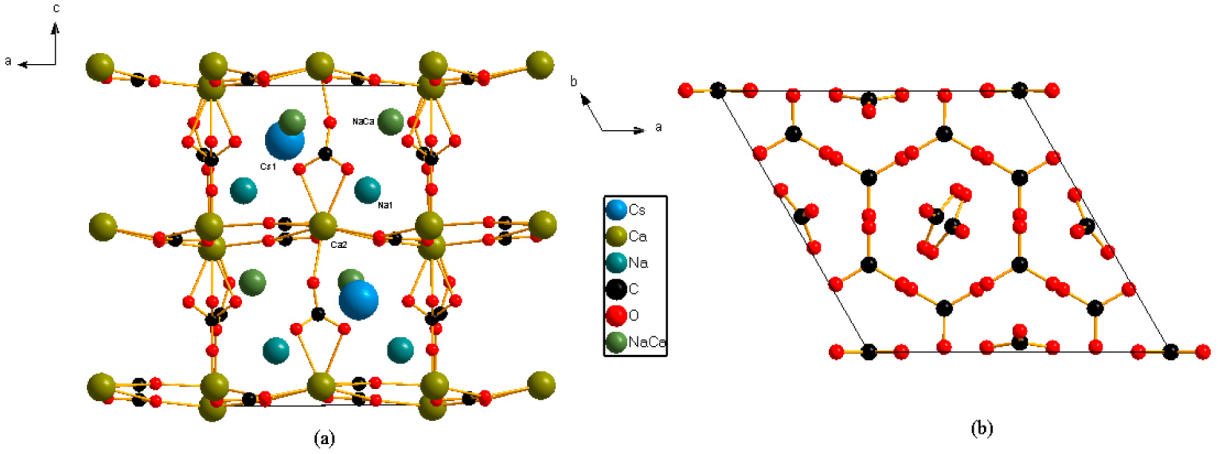

Figure 2. (a) View of the structure of $CsNa_5Ca_5(CO_3)_8$ down the *b* axis. (b) The "flat-lying" and "standing-on-edge" of $[CO_3]^{2-}$ groups in $CsNa_5Ca_5(CO_3)_8$.

First-Principles Calculations. The electronic properties of $Na_4La_2(CO_3)_5$ and $CsNa_5Ca_5(CO_3)_8$ are accomplished by using density functional theory (DFT) calculation with CASTEP code[40] provided by the Material Studio package. Interaction of the electrons with ion cores was represented by the norm-conserving pseudopotentials, and the valence electrons are treated as follows: C $2s^22p^2$, O $2s^22p^4$, Na $2s^22p^63s^1$, Ca $3s^23p^64s^2$, Cs $5s^25p^66s^1$, and La $5d^16s^2$. Generalized gradient approximation (GGA) in the scheme of Perdew–Burke–Eruzerhof (PBE)[41] was used to describe the exchange and correlative potential of electron–electron interactions. The *k*-point of first Brillouin zone was sampled as $2 \times 2 \times 2$ and $2 \times 2 \times 1$ Monkhorst–Pack scheme[42] for $Na_4La_2(CO_3)_5$ and $CsNa_5Ca_5(CO_3)_8$, respectively. Energy cutoff and convergence criteria were set to 750 and 800 eV, respectively, for $Na_4La_2(CO_3)_5$ and $CsNa_5Ca_5(CO_3)_8$. The self-consistent convergence of the total energy was 1.0×10^{-5} eV/atom for $Na_4La_2(CO_3)$ and $CsNa_5Ca_5(CO_3)_8$. The X-ray crystal structure data were used without further optimization. Since the optical properties of mix occupied compound could not be calculated by CASTEP, we designed one of its order structure to estimate $Na_4La_2(CO_3)_5$ and $CsNa_5Ca_5(CO_3)_8$ dielectric function. In addition, for the $CsNa_5Ca_5(CO_3)_8$ compound, we selected the disorder CO_3 plane to be along the ⟨010⟩ direction in the calculation.

RESULTS AND DISCUSSION

Crystal Structure. $Na_4La_2(CO_3)_5$ and $CsNa_5Ca_5(CO_3)_8$ are in the noncentrosymmetric hexagonal space group *P*63*mc*. In both structures, all the C atoms are surrounded by three O atoms to construct planar $[CO_3]$ triangles, and $[CO_3]$ triangles can be classified into two types according to Grice, namely, "flat-lying" and "standing-on-edge."

$Na_4La_2(CO_3)_5$. The crystal structure of $Na_4La_2(CO_3)_5$ consists of isolated CO_3 triangles and complex irregular $[Na_{0.67}La_{0.33}O_{10}]$ and $[NaO_8]$ polyhedra. As regards the structure, Na1 atom is disordered with La1 atom on one crystallographic site, which is coordinated to ten O atoms forming $[Na_{0.67}La_{0.33}O_{10}]$ polyhedra with the range of $Na_{0.67}La_{0.33}$–O bond lengths being from 2.530(6) to 2.775(6) Å. The $[Na_{0.67}La_{0.33}O_{10}]$ polyhedra are connected to each other and to the $[CO_3]$ groups by sharing corners and edges forming a three-dimensional network with channels running through the *c* axis. In these channels the Na2 atoms are situated and are surrounded by eight oxygen atoms with the range of the Na–O bond length being from 2.403(7) to 2.741(7) Å. In terms of $[CO_3]$ planar triangles, the range of C–O bond lengths is between 1.257(6) and1.296(5) Å, and O–C–O bond angles range from 119.80(11) and 120.0(3)°. In this structure, half of the flat-lying $[CO_3]$ groups on the (001) layer aligned antiparallel to the other, resulting in the cancellation of NLO susceptibilities. While $Na_4La_2(CO_3)_5$ exhibits moderate NLO response, it mainly depended on the standing-on-edge $[C3O_3]$ group, which inclined to the *c* axis in approximately the same direction (see Figure 3).

$CsNa_5Ca_5(CO_3)_8$. The structure of $CsNa_5Ca_5(CO_3)_8$ can be described as the standing-on-edge $[CO_3]$ groups connect the adjacent infinite $[CaCO_3]_\infty$ layers in the *ab* plane to construct a

dx.doi.org/10.1021/ic501089f | Inorg. Chem. 2014, 53, 8098–8104

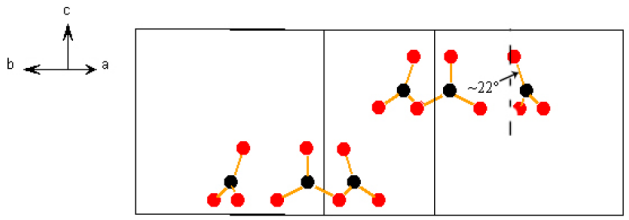

Figure 3. Standing-on-edge $[CO_3]^{2-}$ groups in $Na_4La_2(CO_3)_5$.

framework with four types of channels running parallel to [010] (see Figure 2a). The Na, Cs, and $[Na_{0.67}Ca_{0.33}]$ atoms reside in these channels, respectively, in which Na atoms are situated in an eight-coordination environment with the range of Na−O bond lengths being from 2.387(3) to 2.581(1) Å, Cs atoms are situated in a nine-coordination environment with the range of Cs−O bond lengths being from 3.006(6) to 3.448(4) Å, and $[Na_{0.67}Ca_{0.33}]$ atoms are coordinated to nine O atoms with the range of $Na_{0.67}Ca_{0.33}$−O bond lengths being from 2.437(1) to 2.709(3) Å. In terms of $[C1O_3]$, $[C2O_3]$, and $[C4O_3]$ planar triangles, the range of C−O bond lengths is between 1.232(4) and 1.295(1) Å, and O−C−O bond angles range from 114.6(1)° to 122.7(7)°. Because the O7 atoms were split with a scale factor of 0.33, C3 atoms are coordinated to six O7 atoms and one O1 atom to form a propeller shape along the *c* axis. In the structure, the flat-lying $[CO_3]$ groups in two successive layers present an opposite orientation (see Figure 2b). This arrangement is negative for NLO susceptibilities. The macroscopic SHG effects, however, originated from the standing-on-edge $[CO_3]$ group along the *c* axis. It is regrettable that the standing-on-edge $[C3O_3]$ and $[C4O_3]$ groups are almost arranged oppositely to the *c* direction (see Figure 4), which cancels the d_{33} contribution from the $[C4O_3]$ group. Hence, the SHG effect of $CsNa_5Ca_5(CO_3)_8$ is smaller than that of $Na_4La_2(CO_3)_5$.

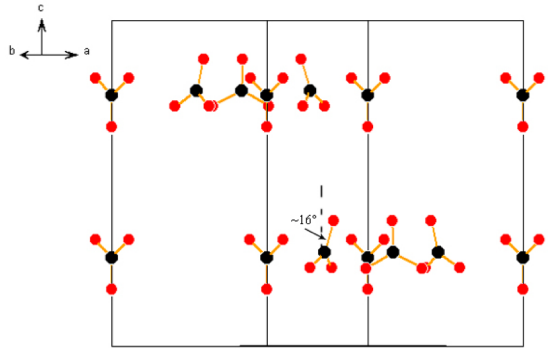

Figure 4. Standing-on-edge $[CO_3]^{2-}$ groups in $CsNa_5Ca_5(CO_3)_8$.

TG Analysis. The thermogravimetric analysis (TGA) curves of $Na_4La_2(CO_3)_5$ and $CsNa_5Ca_5(CO_3)_8$ are shown in Supporting Information, Figure S2. TGA curves of $Na_4La_2(CO_3)_5$ and $CsNa_5Ca_5(CO_3)_8$ exhibit weight losses in three steps and two steps, respectively. The first step in $Na_4La_2(CO_3)_5$, occurring about 400−650 °C, is attributed to the loss (weight %) of 2 mol of CO_2 vapor per mol of $Na_4La_2(CO_3)_5$ (experimental/theoretical = 13.4/13.1). The decomposition reaction is

$$Na_4La_2(CO_3)_5 \rightarrow 2Na_2CO_3 + La_2O_2CO_3 + 2CO_2\ (g)$$

The second step for $Na_4La_2(CO_3)_5$ is the release of 1 mol of CO_2 (experimental/theoretical = 5.9/6.6) from compound $La_2O_2CO_3$, which occurs in the interval of 650−800 °C. The decomposition reaction is

$$La_2O_2CO_3 \rightarrow La_2O_3 + CO_2\ (g)$$

The temperature range of first weight loss for $CsNa_5Ca_5(CO_3)_8$ is between 550 and 800 °C, which is attributed to the release of 5 mol of CO_2 (experimental/theoretical = 23.8/23.7). The decomposition reaction is

$$CsNa_5Ca_5(CO_3)_8 \rightarrow 2.5Na_2CO_3 + 0.5Cs_2CO_3 + 5CaO + 5CO_2\ (g)$$

For the $Na_4La_2(CO_3)_5$ material, the third step corresponds to the decomposition of Na_2CO_3. For the $CsNa_5Ca_5(CO_3)_8$ material, the final step will be the decomposition of Na_2CO_3 and Cs_2CO_3. All of the reaction mechanisms are confirmed by the PXRD at different temperatures (see Figure S3 in the Supporting Information).

Optical Properties. The data of UV−vis diffuse reflectance spectra were collected for all of the titled compounds (see Figure S4 in the Supporting Information). Absorption (*K*/*S*) data were calculated from the following Kubelka—Munk function: $F(R) = (1 - R)^2/2R = K/S$. The study of the optical diffuse reflectance spectra of $Na_4La_2(CO_3)_5$ and $CsNa_5Ca_5(CO_3)_8$ indicated that the optical band gaps for both compounds are approximately 5.29 eV and 5.92 eV, corresponding to the UV cutoff edges that were at ~235 and ~210 nm, respectively, suggesting that all of these crystals were promising for applications in the UV region.

NLO Properties. As shown in Figure 5, according to the rule proposed by Kurtz and Perry, the curves of the SHG signal of $Na_4La_2(CO_3)_5$ and $CsNa_5Ca_5(CO_3)_8$ were consistent with phase-matching behaviors. The measurements of SHG signals of $Na_4La_2(CO_3)_5$ and $CsNa_5Ca_5(CO_3)_8$, selecting the KDP sample as a reference, were found to be approximately 3 and 1 × that of KDP, respectively. These values were proportional to the squares of the nonlinear d_{eff} coefficients. Since the reported d_{36} coefficient for KDP was 0.39 pm/V, the derived d_{eff} coefficients for $Na_4La_2(CO_3)_5$ and $CsNa_5Ca_5(CO_3)_8$ were 1.08 and 0.39 pm/V, respectively.

According to the anionic group theory,[43] owing to the fact that the value of the dipole transition of the intra-atomic transitions within anionic groups was much larger than that of the dipole transition from the cations to the anionic group ($[CO_3]$ in this case), the SHG coefficients should mainly originate from the contribution of anionic group $[CO_3]$. To clearly illustrate the relationship between the anionic group $[CO_3]$ and the NLO properties, the computational method reported in ref 44 was used. Computational details and processes are shown in the Supporting Information, and the calculated results are presented in Table 2.

Assuming that the compounds had similar refractive indices, the localized field (*F*) was equal. According to eqs (2) and (4) in the Supporting Information, we can clearly see that the NLO coefficient $\chi^{(2)}_{ijk}$ is proportional to the structural criterion (*C*) and density of the $[CO_3]$ group (*n*/*V*). The $[CO_3]$ groups in $Na_4La_2(CO_3)_5$ and $CsNa_5Ca_5(CO_3)_8$ had two arrangements, namely, flat-lying and standing-on-edge. The flat-lying $[CO_3]$ groups on the (001) layer in both compounds aligned antiparallel to each other, giving almost no contribution to the *C* factor. Major contribution to the *C* factor mainly

dx.doi.org/10.1021/ic501089f | Inorg. Chem. 2014, 53, 8098−8104

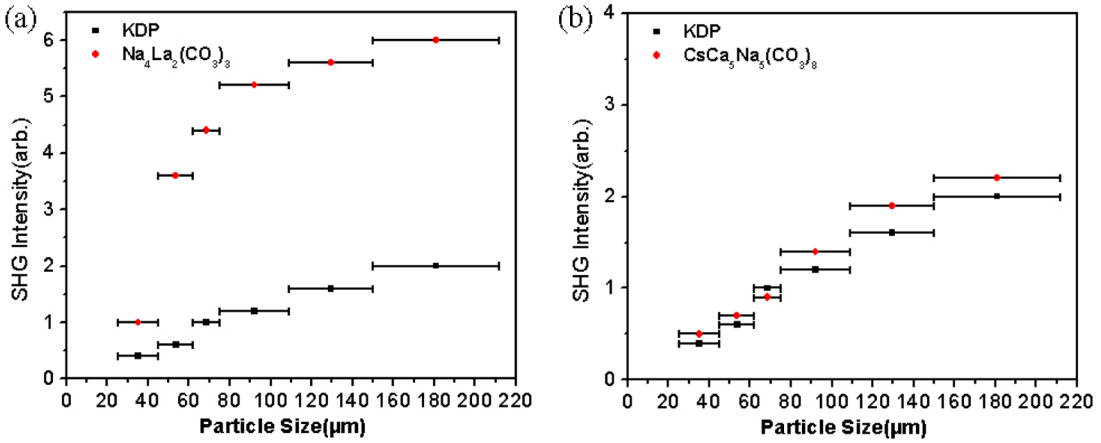

Figure 5. SHG measurements of $Na_4La_2(CO_3)_5$ (a) and $CsNa_5Ca_5(CO_3)_8$ (b) ground crystals (●) with KDP (■) as a reference.

Table 2. NLO Effects of $KSrCO_3F$, $Na_4La_2(CO_3)_5$, and $CsNa_5Ca_5(CO_3)_8$

crystals	SHG coefficient (× KDP)	structural criterion C	density of the $[CO_3]$ group (n/V) (Å^{-3})	$(n/V) \times C$ (Å^{-3})
$KSrCO_3F$[27]	3.33	1	0.0089	0.0089
$Na4La2(CO_3)_5$	3	0.492	0.0160	0.0079
$CsNa5Ca5(CO_3)_8$	1	0.207	0.0143	0.0030

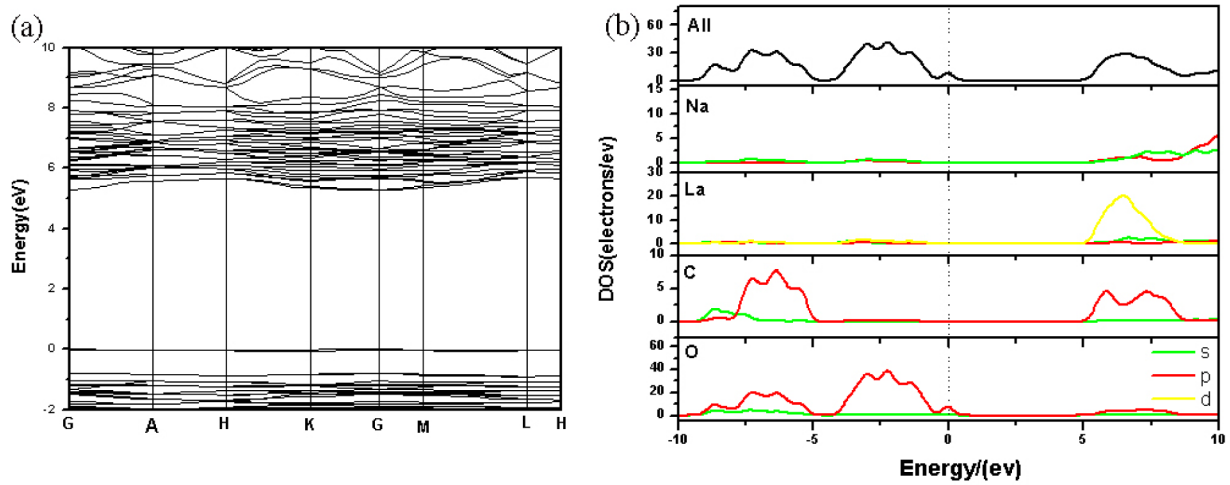

Figure 6. Electronic properties in $Na_4La_2(CO_3)_5$. (a) Band structure. (b) DOS and PDOS.

originated from the standing-on-edge $[CO_3]$ groups along the c axis in both compounds. As shown in Figures 3 and 4, we can clearly see how the C factor is affected by the standing-on-edge $[CO_3]$ groups in both compounds. The six standing-on-edge $[CO_3]$ groups in $Na_4La_2(CO_3)_5$ only exhibited a set of arrangement, which skew toward the c axis by about 22° and had the same direction. This arrangement was conducive to increasing the C factor. Compared with $Na_4La_2(CO_3)_5$, however, the standing-on-edge $[CO_3]$ groups in $CsNa_5Ca_5(CO_3)_8$ had two sets of arrangement, among which six $[CO_3]$ groups skew toward the c axis by about 16° and the other two $[CO_3]$ groups are perfectly aligned to the c direction. Owing to the two sets of arrangement having opposite direction, the standing-on-edge $[CO_3]$ groups in $CsNa_5Ca_5(CO_3)_8$ had a negative contribution to the C factor. The accurate calculated C factors of $Na_4La_2(CO_3)_5$ and $CsNa_5Ca_5(CO_3)_8$ were 0.492 and 0.207, respectively. Because the $Na_4La_2(CO_3)_5$ had not only a larger structural criterion C but also the higher density of the $[CO_3]$ group (0.0160) than that of the $CsNa_5Ca_5(CO_3)_8$ (0.0143), the macroscopic SHG coefficient of $Na_4La_2(CO_3)_5$ is larger than that of $CsNa_5Ca_5(CO_3)_8$. By comparison of the two titled compounds with $KSrCO_3F$, we will further illustrate the relationship between the arrangement and density of NLO-active groups and the macroscopic SHG responses. Although both titled compounds had higher density of $[CO_3]$ groups, the structural factor C of both titled compounds was lower than that of $KSrCO_3F$. Because NLO coefficient $\chi^{(2)}_{ijk}$ is proportional to the density of the $[CO_3]$ group (n/V) and the structural factor (C), the calculated values of $(n/V) \times C$ (Å^{-3}) of $KSrCO_3F$, $Na_4La_2(CO_3)_5$, and $CsNa_5Ca_5(CO_3)_8$ were 0.0089, 0.0079, and 0.0030, respectively, which resulted in the smaller SHG effects of both titled compounds than that of $KSrCO_3F$. The above discussion on the relationship between structure and properties was in accordance with the SHG measurements (see Table 2).

Besides, the contribution of cation for the SHG response was also taken into consideration by calculating the local dipole moments.[45−48] The direction and magnitude of $La(1)_{0.67}Na$-

dx.doi.org/10.1021/ic501089f | Inorg. Chem. 2014, 53, 8098−8104

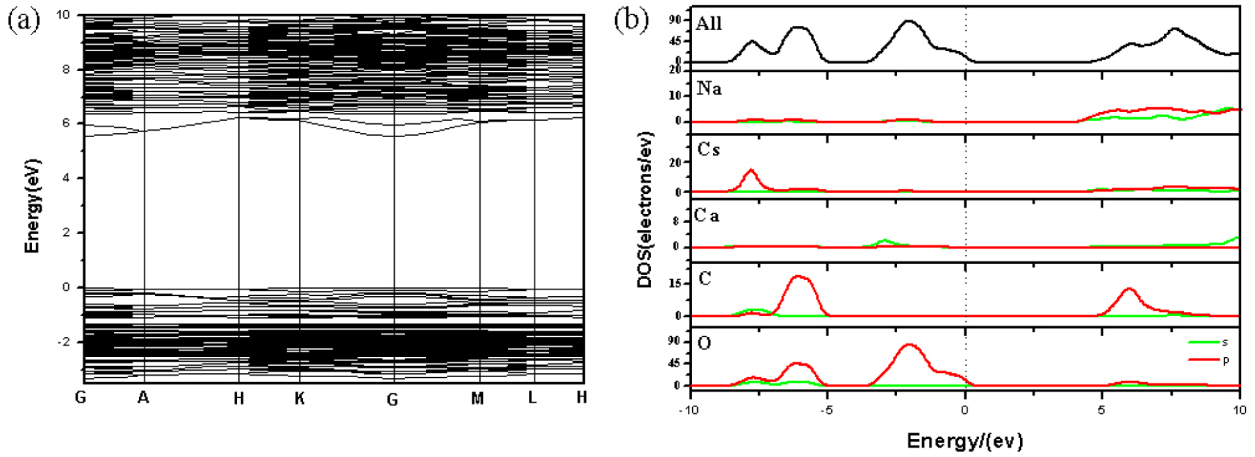

Figure 7. Electronic properties in $CsNa_5Ca_5(CO_3)_8$. (a) Band structure. (b) DOS and PDOS.

$(1)_{0.33}O_{10}$ and $Na(2)O_8$ polyhedra in $Na_4La_2(CO_3)_5$ and $Cs1O_9$, $Na1O_8$, $Na(2)_{0.67}Ca(3)_{0.33}O_9$, $Ca(1)O$, and $Ca(2)O$ polyhedra in $CsNa_5Ca_5(CO_3)_8$ are shown in the Supporting Information (Tables S6 and S7). Clearly, the polarizations of all polyhedras for both compounds were almost canceled along the *x* and *y* axes, and their vector sum was well-enhanced along the *z* axis, which means that the contribution for SHG effect may also partly originate from the combinations of cation polyhedras along the *z* axis. Consequently, according to two aforementioned analysis methods, the SHG effect for both titled compounds may originate from the combination of triangular CO_3 groups and the cation polyhedra.

Theoretical Calculations. The band structures of $Na_4La_2(CO_3)_5$ and $CsNa_5Ca_5(CO_3)_8$ are presented in Figures 6a and 7a. Compounds $Na_4La_2(CO_3)_5$ and $CsNa_5Ca_5(CO_3)_8$ exhibit direct band gaps of 5.288 and 5.572 eV, respectively. Owing to the underestimation of band gap by the DFT method, these calculated values were smaller than the experimental values (5.29 and 5.92 eV).

As we all know, linear and nonlinear optical properties of crystals mainly depend on the states close to the forbidden band. Hence, only the upper region of the valence band (VB) and the bottom of the conduction band (CB) were shown in the total and partial densities of states (DOS and PDOS) of $Na_4La_2(CO_3)_5$ and $CsNa_5Ca_5(CO_3)_8$, respectively (see Figures 6b and 7b). For compounds $Na_4La_2(CO_3)_5$ and $CsNa_5Ca_5(CO_3)_8$, it was obvious that the contribution from the alkaline metal (Cs, Na) or alkaline earth metal (Ca) orbitals can almost be overlooked in these states. On the other hand, for $Na_4La_2(CO_3)_5$, the 4d orbitals of La were 5 eV above the CB minimum. Since the highest VB and the lowest CB were mainly composed of O 2p and C 2p states, the SHG coefficients primarily originate from the contribution of CO_3 polyhedra.

CONCLUSIONS

In summary, two new noncentrosymmetric carbonates ($Na_4La_2(CO_3)_5$ and $CsNa_5Ca_5(CO_3)_8$) have been successfully prepared by hydrothermal reaction. The UV−vis−NIR diffuse reflectance spectroscopy on powder samples of $Na_4La_2(CO_3)_5$ and $CsNa_5Ca_5(CO_3)_8$ indicates that they have a wide transparent region with the short-wavelength absorption edge about 235 and 210 nm, respectively. The NLO properties of $Na_4La_2(CO_3)_5$ and $CsNa_5Ca_5(CO_3)_8$ measured by the method adapted from Kurtz and Perry showed that the compounds exhibited SHG responses of approximately 3 and 1 × that of KH_2PO_4 (KDP) and were phase-matchable in the visible region, respectively. The characteristics of moderate SHG effects and a short UV cutoff edge were favorable in practical applications as UV NLO materials.

ASSOCIATED CONTENT

Supporting Information

Atomic positions, elemental analysis, powder XRD patterns, TG diagrams, diffuse reflectance absorption curves, local dipole moment, and crystal data (CIF). This material is available free of charge via the Internet at http://pubs.acs.org.

AUTHOR INFORMATION

Corresponding Author

*E-mail: nye@fjirsm.ac.cn.

Notes

The authors declare no competing financial interest.

ACKNOWLEDGMENTS

This research was supported by the National Natural Science Foundation of China (Nos. 91222204 and 90922035), Main Direction Program of Knowledge Innovation of Chinese Academy of Sciences (Grant No. KJCX2-EW-H03-03), and Special Project of National Major Scientific Equipment Development of China (No. 2012YQ120060).

REFERENCES

(1) Chen, C. T.; Wu, B. C.; Jiang, A. D.; You, G. M. *Sci. Sin., Ser. B* **1985**, *28*, 235−243.
(2) Chen, C. T.; Wu, Y. C.; Jiang, A. D.; You, G. M.; Li, R. K.; Lin, S. J. *J. Opt. Soc. Am. B* **1989**, *6*, 616−621.
(3) Wu, Y. C.; Sasaki, T.; Nakai, S.; Yokotani, A.; Tang, H. G.; Chen, C. T. *Appl. Phys. Lett.* **1993**, *62*, 2614−2615.
(4) Mori, Y.; Kuroda, I.; Nakajima, S.; Sasaki, T.; Nakai, S. *Appl. Phys. Lett.* **1995**, *67*, 1818−1820.
(5) Wang, S.; Ye, N. *J. Am. Chem. Soc.* **2011**, *133*, 11458−11461.
(6) Wang, S.; Ye, N.; Li, W.; Zhao, D. *J. Am. Chem. Soc.* **2010**, *132*, 8779−8786.
(7) Wu, H.; Pan, S.; Poeppelmeier, K. R.; Li, H.; Jia, D.; Chen, Z.; Fan, X.; Yang, Y.; Rondinelli, J. M.; Luo, H. *J. Am. Chem. Soc.* **2011**, *133*, 7786−7790.
(8) Keszler, D. A. *Curr. Opin. Solid State Mater. Sci.* **1999** *4*, 155−162.

(9) Xu, X.; Hu, C. L.; Kong, F.; Zhang, J. H.; Mao, J. G.; Sun, J. *Inorg. Chem.* **2013**, *52*, 5831−5837.
(10) Huang, H.; Liu, L.; Jin, S.; Yao, W.; Zhang, Y.; Chen, C. *J. Am. Chem. Soc.* **2013**, *135*, 18319−18322.
(11) Yan, X.; Luo, S.; Lin, Z.; Yao, J.; He, R.; Yue, Y.; Chen, C. *Inorg. Chem.* **2014**, *53*, 1952−1954.
(12) Wu, H.; Yu, H.; Yang, Z.; Hou, X.; Su, X.; Pan, S.; Poeppelmeier, K. R.; Rondinelli, J. M. *J. Am. Chem. Soc.* **2013**, *135*, 4215−4218.
(13) Huang, H. W.; Yao, J. Y.; Lin, Z. S.; Wang, X. Y.; He, R.; Yao, W. J.; Zhai, N. X.; Chen, C. T. *Angew. Chem., Int. Ed.* **2011**, *50*, 9141.
(14) Sun, C. F.; Hu, C. L.; Xu, X.; Yang, B. P.; Mao, J. G. *J. Am. Chem. Soc.* **2011**, *133*, 5561−5572.
(15) Chang, H. Y.; Kim, S. H.; Ok, K. M.; Halasyamani, P. S. *J. Am. Chem. Soc.* **2009**, *131*, 6865−6873.
(16) Chang, H. Y.; Kim, S. H.; Ok, K. M.; Halasyamani, P. S. *Chem. Mater.* **2009**, *21*, 1654−1662.
(17) Wu, H.; Yu, H.; Pan, S.; Huang, Z.; Yang, Z.; Su, X.; Poeppelmeier, K. R. *Angew. Chem., Int. Ed.* **2013**, *52*, 3406−3410.
(18) Chen, C. T.; Wu, Y. C.; Li, R. K. *Int. Rev. Phys. Chem.* **1989**, *8*, 65−91.
(19) Chen, C. T.; Liu, G. Z. *Annu. Rev. Mater. Sci.* **1986**, *16*, 203−243.
(20) Chen, C. T. *Sci. Sin. (Engl. Ed.)* **1979**, *22*, 756.
(21) Mei, L. F.; Wang, Y. B.; Chen, C. T.; Wu, B. C. *J. Appl. Phys.* **1993**, *74*, 7014−7015.
(22) Chen, C. T.; Wang, Y. B.; Wu, B. C.; Wu, K. C.; Zeng, W. L.; Yu, L. H. *Nature* **1995**, *373*, 322−324.
(23) Aka, G.; KahnHarari, A.; Mougel, F.; Vivien, D.; Salin, F.; Coquelin, P.; Colin, P.; Pelenc, D.; Damelet, J. P. *J. Opt. Soc. Am. B* **1997**, *14*, 2238−2247.
(24) Belokoneva, E. L.; Azizov, A. V.; Leonyuk, N. I.; Simonov, M. A. *J. Struct. Chem.* **1981**, *22*, 476−478.
(25) Mills, A. D. *Inorg. Chem.* **1962**, *1*, 960−961.
(26) Ballman, A. A. *Am. Mineral.* **1962**, *47*, 1380−1833.
(27) Zou, G.; Ye, N.; Huang, L.; Lin, X. *J. Am. Chem. Soc.* **2011**, *133*, 20001−20007.
(28) Tran, T. T.; Halasyamani, P. S. *Inorg. Chem.* **2013**, *52*, 2466−2473.
(29) Luo, M.; Ye, N.; Zou, G.; Lin, C.; Cheng, W. *Chem. Mater.* **2013**, *25*, 3147−3153.
(30) Zou, G.; Huang, L.; Ye, N.; Lin, C.; Cheng, W.; Huang, H. *J. Am. Chem. Soc.* **2013**, *135*, 18560−18566.
(31) Luo, M.; Lin, C.; Zou, G.; Ye, N.; Cheng, W. *CrystEngComm* **2014**, *32*, 4414−4421.
(32) Grice, J. D.; VanVelthuizen, J.; Gault, R. A. *Can. Mineral.* **1994**, *32*, 405−414.
(33) Grice, J. D.; Chao, G. Y. *Am. Mineral.* **1997**, *82*, 1255−1260.
(34) Grice, J. D.; Gault, R. A.; Van Velthuizen, J. *Can. Mineral.* **1997**, *35*, 181−187.
(35) Sheldrick, G. M. *Acta Crystallogr., Sect. A* **2008**, *64*, 112−122.
(36) Spek, A. L. *J. Appl. Crystallogr.* **2003**, *36*, 7−13.
(37) Kubelka, P.; Munk, F. Z. *Tech. Phys.* **1931**, *12*, 593−601.
(38) Tauc, J. *Mater. Res. Bull.* **1970**, *5*, 721−730.
(39) Kurtz, S. K.; Perry, T. T. *J. Appl. Phys.* **1968**, *39*, 3798−3813.
(40) Clark, S. J.; Segall, M. D.; Pickard, C. J.; Hasnip, P. J.; Probert, M. J.; Refson, K.; Payne, M. C. *Z. Kristallogr.* **2005**, *220*, 567−570.
(41) Perdew, J. P.; Burke, K.; Ernzerhof, M. *Phys. Rev. Lett.* **1996**, *77*, 3865−3868.
(42) Monkhorst, H. J.; Pack, J. D. *Phys. Rev. B* **1976**, *13*, 5188−5192.
(43) Chen, C.; Lin, C.; Wang, Z. *Appl. Phys. B: Lasers Opt.* **2005**, *80*, 1−25.
(44) Ye, N.; Chen, Q. X.; Wu, B. C.; Chen, C. T. *J. Appl. Phys.* **1998**, *84*, 555−558.
(45) Eckardt, R. C.; Masuda, H.; Fan, Y. X.; Byer, R. L. *IEEE J. Quantum Electron.* **1990**, *26*, 922−933.
(46) Godby, R. W.; Schluter, M.; Sham, L. J. *Phys. Rev. B: Condens. Matter Mater. Phys.* **1987**, *36*, 6497−6500.
(47) Terki, R.; Bertrand, G.; Aourag, H. *Microelectron. Eng.* **2005**, *81*, 514−523.
(48) Wang, G.; Luo, M.; Ye, N.; Lin, C.; Cheng, W. *Inorg. Chem.* **2014**, *53*, 5222−5228.